International Journal of Solids and Structures 51 (2014) 3973–3986

Contents lists available at ScienceDirect

International Journal of Solids and Structures

journal homepage: www.elsevier.com/locate/ijsolstr

The *LS1* model for delamination propagation in multilayered materials at $0^\circ/\theta^\circ$ interfaces: A comparison between experimental and finite elements strain energy release rates

Achille Lerpiniere *, Jean-François Caron, Alberto Diaz Diaz, Karam Sab

Université Paris-Est, Laboratoire Navier (École des Ponts ParisTech, IFSTTAR, CNRS), École des Ponts Paristech, 6 et 8 avenue Blaise Pascal, 77455 Marne-la-Vallée, France

ARTICLE INFO

Article history:
Received 9 December 2013
Received in revised form 20 June 2014
Available online 14 August 2014

Keywords:
Multilayer
Layerwise model
Delamination criterion
Interlaminar stresses

ABSTRACT

The aim of this paper is to analyze delaminated multilayered plates under classical loads using an alternative model to the existing three-dimensional finite element methods (3D-FEM). The proposed alternative model, named *LS1*, is a layerwise stress model proving significantly less computationally expensive while accurate and efficient. In particular this paper uses experimental data from different simple test specimens in a finite element code, which is based on *LS1*, in order to calculate strain energy release rates (SERR) in different modes of delamination. The focus is on two types of delaminated interfaces 0°/0° and 0°/45°. The obtained SERR results are in very good agreement with the experimental values and, in the case of mixed-mode delamination, they are as accurate as the SERR obtained by 3D-FE models. The other interesting property of the *LS1* model is the very fast calculation speed as the SERR can be analytically deduced from interfacial stresses. This relation which only depends on the stacking sequence and the position of delamination is presented.

1. Introduction

The use of composite materials has increased in the last decades. Different types of damage mechanisms can occur and lead to the ruin of the structure: from intralaminar damage such as fiber breakage, matrix cracking, fiber matrix debonding or even fiber kinking to interlaminar damage such as delamination which is often the critical failure mode in those structures. This failure mode can provoke stiffness decrease and strength degradation, which in turn may lead to partial or complete failure of the composite structure. The study of delamination initiation and propagation is thus quite essential when designing multilayered structures.

Several conditions can induce delamination: external impact, stress concentration in open-hole plate, or interlaminar stress at free edges.

Various methods, viewpoints and criteria exist to take into account this phenomenon. Some studies focus on damage mechanics with the concept of imperfect interface and cohesive zone models to take into account delamination (Allix and Ladevèze, 1992; Allix et al., 1998; Greco et al., 2002; Borg et al., 2002; Harper and Hallett, 2008; Qiu et al., 2001; Camanho et al., 2003). In these methods, which are especially effective for the delamination nucleation, the delamination state corresponds to total damage of the imperfect interface. Some others methods use energy considerations and fracture mechanics by defining delamination as the propagation of a crack between the two surrounding layers of the delaminated interface (Davidson, 1990; Larsson, 1991; Nilsson, 1993; Ousset, 1999; Diaz et al., 2007). The virtual crack closure technique (VCCT) (Krueger, 2004), the virtual crack extension (VCE) (Hwang et al., 1998) and the J-integral techniques (Rice, 1968) are used for numerical modeling of delamination based on energy criteria along with finite element method (FEM). Other delamination criteria are directly either stress or strain based and use threshold values or equations containing mainly out-of-plane properties (Orifici et al., 2008; Diaz et al., 2007). The major difficulty then is that those criteria often depend on stacking sequence, ply orientation, or ply thickness (Andersons and König, 2004; Davidson et al., 1996; Lachaud et al., 1998).

It appears many models have been proposed to foresee delamination in composite structures. However, on account of the intricacy of stress fields at free edges and crack tips, it is still necessary to develop an efficient and accurate method to model the initiation and the propagation of delamination. The nucleation of delamination and its evolution is a complex process, clearly the problem at hand is three-dimensional. Diverse 3D approaches can be found in

* Corresponding author. Tel.: +33 1 64153735; fax: +33 1 64153741.
E-mail addresses: achille.lerpiniere@enpc.fr (A. Lerpiniere), caron@enpc.fr (J.-F. Caron), alberto.diaz@cimav.edu.mx (A. Diaz Diaz), karam.sab@enpc.fr (K. Sab).

http://dx.doi.org/10.1016/j.ijsolstr.2014.07.018
0020-7683/

literature for the study of delamination. In finite element simulations, in order to capture precisely the stress concentration at free edges or crack tips, a substantial number of elements must be placed through the thickness of the laminate in their vicinity. A non-local criterion based on a ply scale characteristic length (Whitney and Nuismer, 1974) or volume (Hochard et al., 2007; Tan, 1988) implemented in a finite element approach has also been proposed to avoid this by calculating an effective stress integrated on this length or volume. However then different tests are needed to identify the size of this characteristic dimension which depends on the structure of the ply. Special crack tip elements may also be employed to better estimate the stress singularity with a lower number of elements (Yu and Davidson, 2001), however the stress solution had still better be handled with care. Thus, the finite element calculation may get very large and computationally expensive which is not really inviting when designing complex composite structures.

As a result, effective one-dimensional or two-dimensional approaches are also needed for the study of delamination cases. The beam (1D) and plate (2D) theories have been broadly employed for the delamination analysis of laminated composites.

The delamination in multilayered structures was firstly modeled using classical laminate theory (CLT) in which transverse shears are not taken into account, especially when considering classical test samples such DCB (double-cantilever beam), ELS (end loaded split) and MMF (mixed-mode flexure) (Kinloch et al., 1993; Hashemi et al., 1990; Williams, 1989). The first-order shear deformation theories (FSDT), which add a shear correction factor to the CLT, have also been employed for delamination analyzes (Zhang et al., 1999; Szekrenyes, 2013a). Bruno et al. (2005) used an assembly of FSDT plate elements connected by elastic interfaces and the SERR are given in terms of interface variables and of plate stress resultant discontinuities. Shen and Grady (1992) studied the dynamic response of a delaminated composite beam by using the Timoshenko beam theory. Chattopadhyay (1994) and Szekrenyes (2013b) established a higher order theory for taking into account delamination in composite plates and shells with moderate thickness. Although results of higher order theories are globally exact, the stress continuity condition at non delaminated interfaces is not verified.

To solve this problem, and go further in the displacement or stress field description in the thickness of a laminated plate, the so-called layerwise description are very often used. Fields are described at the ply level, and the interfaces between plies appear naturally. Many layerwise approaches where displacements or/and stresses are approximated by polynomial or sinus functions (see a review in Carrera (2004) and following details) exist. In most cases, these were presented to improve the accuracy of non-delaminated plate descriptions. While for delamination phenomena, some developments were proposed. Barbero and Reddy (1991) and later Moorthy and Reddy (1998) firstly developed a layerwise method for the modeling of delamination in multilayered structures. Lee (2000) used a layerwise theory to analyze the free vibration response of a delaminated multilayered beam. In Cho (2001) and Oh et al. (2008), a degraded layerwise theory, inducing fewer unknowns and belonging to the so-called Zig-Zag family (see for example Murakami, 1986) is used for studying multi-delaminated composite plates. Zou et al. (2002) introduced a two-dimensional model, as a combination of sub-laminates connected through their interfaces, to allow for the progressive interlaminar delamination in multi-layered structures. Kim et al. (2003) proposed a new generalized layerwise method to describe the incidence of delamination on the dynamic response of multi-layered specimens with arbitrary stacking sequences.

The present approach can be indexed in the layerwise family, the objective of this paper is then to present an efficient and accurate alternative to 3D methods for analyzing delaminated multilayered materials, here studied under classical loads in Mode I and/or II. The layerwise model proposed is a stress model, previously called the *multiparticle model of multilayered materials (M4)* (see Naciri et al., 1998; Carreira et al., 2002; Diaz et al., 2002; Caron et al., 2006 Dallot and Sab, 2008; Diaz and Caron, 2006b; Nguyen and Caron, 2006). Referring to Carrera's nomenclature (Carrera, 2004), the M4 model was renamed *LS1* model (layerwise stress approach with first-order membrane stress approximations per layer in the thickness direction (Thai et al., 2013)). In this model, each layer appears as a Reissner–Mindlin plate and the different layers are connected with interfacial stresses which are considered as generalized stresses of the model. Out-of-plane shear and normal stresses continuity is thus achieved at the interfaces. The principal dissimilarity between the *LS1* model and other existing layerwise models is that, in most cases, the layerwise models are either displacement or mixed stress-displacement approaches whereas the *LS1* model, directly inspired from Pagano's model (Pagano, 1978), is a pure layerwise stress approach where there is no preliminary hypothesis on displacement fields.

The analytical solutions of the *LS1* model for uncracked symmetric composites under uniaxial loading were obtained by Naciri et al. (1998) and validated by Carreira et al. (2002) in comparison with finite elements results. A finite element method *MPFEAP* (Multi-Particular Finite Element Program), based on our *LS1* model was implemented Nguyen and Caron (2006) in the software GiD. GiD is a pre and postprocessor for numerical simulations developed in Spain in Universitat Politécnica de Catalunya.

Since this layer-wise model allows to access very directly and without any post-processing the values of the interfacial shears and normal stresses, it is easy to use these interfacial stresses to predict delamination. Analytical developments for the modeling of delamination due to edge effects (mode III) were proposed by Diaz et al. (2007) and Saeedi et al. (2012a). Saeedi et al. (2012a) showed that, for test cases with invariance such as the delamination problem is 1D, initiation of delamination (mode III) can be well predicted using a twofold strength and toughness criterion while delamination propagation is well described using an energy criterion.

The present study investigates the capability of the *LS1* model to describe delamination also for mode I, II and mixed mode I/II. To check the relevance of the results, comparisons are made with existing experimental data. A numerical strategy using our *MPFEAP* software is proposed in this study instead of the analytical one presented in previous papers. It allows a full analysis of complex structures as delaminated symmetric or asymmetric multilayered plates. It reduces drastically computation time compared to 3D finite elements and cohesive zone method (CZM) as it uses 2D plate finite elements. Results from *MPFEAP* code based on *LS1* model will be compared to experimental and 3D finite elements results from Prombut et al. (2006). Test cases were performed on DCB (double cantilever beam), ELS (end loaded split), ADCB (asymmetric double cantilever beam) and MMF (mixed-mode flexure) both UD and MD with 0°/0° and 0°/45° delaminated interfaces. The fracture toughness of these interfaces were calculated with the model *LS1* by using the fact that this approach permits to deduce analytically mode separation from the interfacial stresses.

2. Description of the *LS1* model

The model *LS1*, initially developed for calculating interfacial stresses, Carreira et al. (2002), is specifically devoted to the study of the interface phenomena, delamination initiation or sliding. In the initial formulation (for prepregs studies), interfaces are considered as infinitely thin, perfect (out of-plane stresses continuity, interface infinitely rigid) and the applications used interfacial

stresses for criterion proposals (Caron et al., 2006). But such an approach reaches its own limit very quickly, since the interfaces can be more complex (thicker, with their own behavior, elastoplastic...). There are several ways to manage such interface specificities. The 3D-FEM is once again not the most adapted model, since the interface concentrates high gradients (even singularities) in a weak dimension with regard to those of the layers. It is therefore difficult to use acceptable meshing for both adherends and a thin interface. From a numerical point of view, it leads to problems with too large extensions. Consequently, it is classical to represent joints (with weak thickness and often weak rigidity) with cohesive elements, and to develop specially interface finite elements, with no thickness, which link stresses in the element and displacements close to the interface. A damage model is generally introduced to create delamination.

In *LS1* layerwise approach, several steps were taken in this sense and are detailed below. Firstly, for the study of delamination in a cross ply laminate, Caron et al. (2006), the inelastic behavior of a non-elastic interface was introduced as a non-elastic strain in the analytical model permitting the sliding between two layers of composite as experimentally observed on edges of specimens with an optical microscope. An elastoplastic behavior was adopted to describe the non-elastic relation between generalized interlaminar stresses and generalized displacement discontinuities across the interface. The described interface is not yet really physical since it has not its own behavior. For thicker and more elastoplastic interfaces such as structural bonding (for example joints in wood-concrete beams), a more representative behavior of such an interface was introduced in the model in Duong et al. (2011). Then, the *LS1* model makes possible to describe directly the interface local phenomena and to determine the level of stresses, and the elastic or plastic sliding which can be found in connected or bonded systems while keeping the layerwise plate strategy. Although the *LS1* model provides satisfying and useful *finite* estimations of 3D fields, in the vicinity of singularities (particularly near free edges or crack tips) its results are not exactly those delivered by detailed 3D analysis since they are obtained after integration of the 3D-fields along the thickness of the plies. In order to, reassure users on the relevance of these estimations, and enhance the local estimations, a refinement mesh strategy called *refined LS1* was proposed in Saeedi et al. (2012b). In this way, the accuracy of the model increases as much as needed, and the convergence toward 3D solution is definitely proved. In the following paragraph, the description of the model and the main governing equations are briefly summarized, the different interface models are detailed, the 2D-FEM will be presented in paragraph 2.4.2.

In this section, the formulation of the *LS1* model (layerwise stress model with first-order membrane stress approximation per layer (Thai et al., 2013)), previously called *M4-5n* model (while 5 DOF per layer), is briefly presented. In the next sections, this model will be used to solve the delamination problem in composite laminates under classical loads in mode I and/or II and compared with experimental and 3D finite elements results from Prombut et al. (2006).

2.1. Description and notations

The multilayered plate is then composed of n orthotropic elastic layers bonded together (Fig. 1). In the following formulation, x and y represent the in-plane directions and z is the thickness coordinate.

- Each layer i, thickness e^i, is bounded by the lower surface h_i^- and the top surface h_i^+. The average surface is noted by $\bar{h}_i$. Between two adjacent layers i and $i+1$, the adhesive has a thickness $e^{i,i+1}$.
- The volume occupied by the plate is $\Omega = \omega \times [h_1^-, h_n^+]$.
- The superscripts i and $j, j+1$ indicate layer i and the interface between layers j and $j+1$ ($i = 1 \dots n$ and $j = 1 \dots n-1$).
- The Greek subscripts $\alpha, \beta, \gamma, \delta$ indicate the components on the (x, y) plane and are assigned the values 1 and 2. Subscript 3 indicates the normal direction z.
- Tensors, matrices and vectors are expressed in bold face characters.
- $\sigma_{\alpha\beta}(x,y,z)$ are the in-plane stress components, $\sigma_{\alpha z}(x,y,z)$ the 2 transverse shear stresses, $\sigma_{zz}(x,y,z)$ the normal stress.
- $u_{\alpha\beta}(x,y,z)$ are the in-plane 3D displacement components, $U_z(x,y,z)$ the vertical component.
- $N^i_{\alpha\beta}(x,y)$, $M^i_{\alpha\beta}(x,y)$, $Q^i_{\alpha}(x,y)$, $\tau^{i,i+1}_{\alpha}(x,y)$ and $\nu^{i,i+1}(x,y)$ are the generalized stresses, respectively in-plane stress, moment and shear resultants of layer i.
- $\varepsilon^i_{\alpha\beta}(x,y)$, $\chi^i_{\alpha\beta}(x,y)$, $d^i_{\Phi_\alpha}(x,y)$, $D^{i,i+1}_{\alpha}(x,y)$ and $D^{i,i+1}_{z}(x,y)$ are the respectively associated generalized strains of layer i.
- $U^i_\alpha(x,y), U^i_z(x,y), \Phi^i_\alpha(x,y)$ are the 5 generalized displacements, respectively, 2 in-plane displacements, a vertical one, and 2 rotations, for layer i.
- $S^i_{\alpha\beta\gamma\delta}$ the in-plane elastic compliance components of the layer i, $S^i_{\alpha 3\beta 3} = S^i_{Q_{\alpha\beta}}$ the transverse shear components, and $S^i_{3333} = S^i_\nu$ the normal component of layer i.
- $\gamma_x^{k,k+1}(x,y)$, $\gamma_y^{k,k+1}(x,y)$ and $\gamma_z^{k,k+1}(x,y)$ are three local interface displacements or slips at an imperfect interface $k, k+1$, elastic or delaminated interface for instance.
- $k_x^{k,k+1}, k_y^{k,k+1}$ and $k_z^{k,k+1}$ represent the stiffnesses of an elastic interface $k, k+1$.

2.2. Generalized stresses and 3D stress field

As explained, the *LS1* model is a layerwise model with stress field approximations. Indeed, this model presents a stress approach based on Pagano's model (Pagano, 1978), in which there is no hypothesis on displacement fields. In this model, the 3D stress components are considered as polynomial functions of z whose coefficients are expressed in terms of generalized stresses of the model. The in-plane stress components $\sigma_{\alpha\beta}$ are chosen as

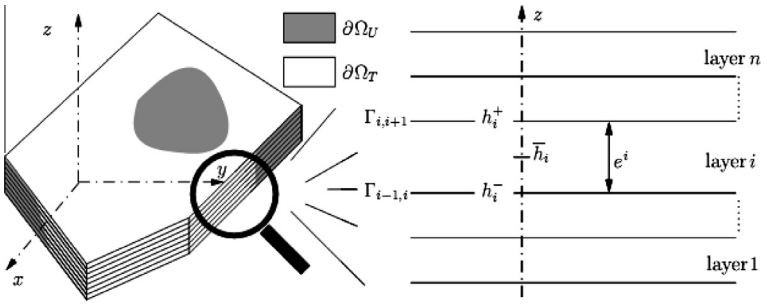

Fig. 1. Description of the laminate.

linear functions of z. According to the 3D equilibrium equations, the shear stresses $\sigma_{\alpha z}$ and the normal stress σ_{zz} are respectively quadratic and cubic polynomial functions of z. The generalized internal stresses are defined as follows ($\alpha, \beta \in \{x, y\}$):

- Respectively:

$$N^i_{\alpha\beta}(x,y) = \int_{h^i_-}^{h^i_+} \sigma_{\alpha\beta}(x,y,z)dz \tag{2.1}$$

$$M^i_{\alpha\beta}(x,y) = \int_{h^i_-}^{h^i_+} (z-\bar{h}^i)\sigma_{\alpha\beta}(x,y,z)dz \tag{2.2}$$

$$Q^i_{\alpha}(x,y) = \int_{h^i_-}^{h^i_+} \sigma_{\alpha z}(x,y,z)dz \tag{2.3}$$

- Interlaminar shear and normal stresses at interface $i, i+1$:

$$\tau^{i,i+1}_{\alpha}(x,y) = \sigma^i_{\alpha z}(x,y,h^i_+) = \sigma^{i+1}_{\alpha z}(x,y,h^{i+1}_-) \tag{2.4}$$

$$v^{i,i+1}(x,y) = \sigma^i_{zz}(x,y,h^i_+) = \sigma^{i+1}_{zz}(x,y,h^{i+1}_-) \tag{2.5}$$

The interlaminar stresses at interfaces are unknowns of the model. Therefore, the stress continuities at the interfaces are automatically satisfied and the interlaminar stresses can be evaluated directly without any postprocessing. If needed, the distributions of the 3D stresses can be calculated across the thickness of the layers. The 3D stress components are expressed in terms of the generalized stresses of the model as described in Saeedi et al. (2012a).

2.3. Generalized displacements and generalized strains

Since the *LS1* model is a layerwise stress approach, there is no hypothesis on the form of the displacement fields and the displacements stem from the model. By introducing the assumed stress fields into the Hellinger–Reissner functional (Reissner, 1950) and integrating with respect to z over the thickness of each layer, the expressions of generalized displacements are deduced. These generalized displacements are in fact weighted-averages of the 3D displacements (see Naciri et al., 1998; Carreira et al., 2002, for more details). In this way, five kinematic fields, 2 in-plane displacements $U^i_\alpha(x,y)(\alpha = 1,2)$, a vertical displacement $U^i_z(x,y)$ and two rotations $\Phi^i_\alpha(x,y)(\alpha = 1,2)$ are introduced for each layer i:

$$U^i_\alpha(x,y) = \frac{1}{e^i}\int_{h^i_-}^{h^i_+} U_\alpha(x,y,z)dz \tag{2.6}$$

$$U^i_z(x,y) = \frac{1}{e^i}\int_{h^i_-}^{h^i_+} U_z(x,y,z)dz \tag{2.7}$$

$$\Phi^i_\alpha(x,y) = \frac{12}{(e^i)^2}\int_{h^i_-}^{h^i_+} \frac{z-\bar{h}^i}{e^i} U_\alpha(x,y,z)dz \tag{2.8}$$

Generalized strains which are deduced from the generalized displacements, are associated with the generalized stresses so that they appear as the energy conjugate to the generalized stresses in the Hellinger–Reissner functional. They are defined as follows:

$$\varepsilon^i_{\alpha\beta} = \frac{1}{2}\left(U^i_{\alpha,\beta} + U^i_{\beta,\alpha}\right) \tag{2.9}$$

$$\chi^i_{\alpha\beta} = \frac{1}{2}\left(\Phi^i_{\alpha,\beta} + \Phi^i_{\beta,\alpha}\right) \tag{2.10}$$

$$d^i_{\Phi_\alpha} = \Phi^i_\alpha + U^i_{z,\alpha} \tag{2.11}$$

$$D^{i,i+1}_\alpha = U^{i+1}_\alpha - U^i_\alpha - \left(\frac{e^i}{2}\Phi^i_\alpha + \frac{e^{i+1}}{2}\Phi^{i+1}_\alpha\right) \tag{2.12}$$

$$D^{i,i+1}_z = U^{i+1}_z - U^i_z \tag{2.13}$$

Accordingly, the generalized strains $\varepsilon^i_{\alpha\beta}$, $\chi^i_{\alpha\beta}$, $d^i_{\Phi_\alpha}$, $D^{i,i+1}_\alpha$ *and* $D^{i,i+1}_z$ are associated, respectively, with the generalized stresses $N^i_{\alpha\beta}$, $M^i_{\alpha\beta}$, Q^i_α, $\tau^{i,i+1}_\alpha$ and $v^{i,i+1}$.

2.4. Constitutive and equilibrium equations

The derivation of the Hellinger–Reissner functional with respect to generalized stresses yields the constitutive equations of the model.

Constitutive relations for layer i:

- Membrane and in-plane shear:

$$\varepsilon^i_{\alpha\beta} = \frac{1}{e^i}S^i_{\alpha\beta\gamma\delta}N^i_{\gamma\delta} \tag{2.14}$$

- Bending and torsion:

$$\chi^i_{\alpha\beta} = \frac{12}{(e^i)^3}S^i_{\alpha\beta\gamma\delta}M^i_{\gamma\delta} \tag{2.15}$$

- Out-of-plane shear:

$$d^i_{\Phi_\alpha} = \frac{6}{5e^i}S^i_{Q_{\alpha\beta}}Q^i_\beta - \frac{1}{10}S^i_{Q_{\alpha\beta}}\left(\tau^{i-1,i}_\beta + \tau^{i,i+1}_\beta\right) \tag{2.16}$$

Constitutive relations for interface $i, i+1$:

- Interlaminar shear stress:

$$\begin{aligned} D^{i,i+1}_\alpha = &-\frac{1}{10}\left(S^i_{Q_{\alpha\beta}}Q^i_\beta + S^{i+1}_{Q_{\alpha\beta}}Q^{i+1}_\beta\right) \\ &-\frac{1}{30}\left(e^i S^i_{Q_{\alpha\beta}}\tau^{i-1,i}_\beta + e^{i+1}S^{i+1}_{Q_{\alpha\beta}}\tau^{i+1,i+2}_\beta\right) \\ &+\frac{2}{15}\left(e^i S^i_{Q_{\alpha\beta}} + e^{i+1}S^{i+1}_{Q_{\alpha\beta}}\right)\tau^{i,i+1}_\beta \end{aligned} \tag{2.17}$$

- Interlaminar normal stress:

$$\begin{aligned} D^{i,i+1}_z = &\frac{9}{70}\left(e^i S^i_v v^{i-1,i} + e^{i+1}S^{i+1}_v v^{i+1,i+2}\right) \\ &+\frac{13}{35}\left(e^i S^i_v + e^{i+1}S^{i+1}_v\right)v^{i,i+1} \end{aligned} \tag{2.18}$$

where $S^i_{\alpha\beta\gamma\delta}$, $S^i_{Q_{\alpha\beta}}$ and S^i_v are components of the compliance matrix of layer i as expressed in Saeedi et al. (2012a).

The derivation of the Hellinger–Reissner functional with respect to generalized displacements leads to the equilibrium equations. Since there are 5 generalized displacements per layer, 5 equilibrium equations $(\alpha, \beta = 1,2)$, are obtained for each layer i:

$$N^i_{\alpha\beta,\beta} + \tau^{i,i+1}_\alpha - \tau^{i-1,i}_\alpha = 0 \tag{2.19}$$

$$M^i_{\alpha\beta,\beta} + \frac{e^i}{2}\left(\tau^{i,i+1}_\alpha + \tau^{i-1,i}_\alpha\right) - Q^i_\alpha = 0 \tag{2.20}$$

$$Q^i_{\beta,\beta} + v^{i,i+1} - v^{i-1,i} = 0. \tag{2.21}$$

2.5. LS1 for delamination

In the previous developments of the *LS1* model, the interfaces were considered as perfect and interface displacements were only due to the elastic generalized displacements in the neighboring layers. Now, if the role of physical interfaces has to be specifically

taken into account (elastic or plastic sliding (Diaz et al., 2002), thick elastic or plastic interface (Duong et al., 2011)), the interface behavior Eqs. (2.17) and (2.18) and (2.13) may highlight this new complexity.

2.5.1. Interface formulation

Thus, in these Eqs. (2.17) and (2.18), generalized elastic interface displacements may legitimately be expressed for $i = 1, 2, 3$, as interface generalized displacements $D_\alpha^{k,k+1}(x,y)$ and $D_z^{k,k+1}(x,y)$ (as defined in (2.12) and (2.13)), minus $\gamma_i^{k,k+1}$ which represent local interface displacements (or slips) due to an own interface behavior:

- Interlaminar shear stress:

$$D_\alpha^{k,k+1} - \gamma_\alpha^{k,k+1} = -\frac{1}{10}\left(S_{Q_{\alpha\beta}}^k Q_\beta^k + S_{Q_{\alpha\beta}}^{k+1} Q_\beta^{k+1}\right) - \frac{1}{30}\left(e^k S_{Q_{\alpha\beta}}^k \tau_\beta^{k-1,k} + e^{k+1} S_{Q_{\alpha\beta}}^{k+1} \tau_\beta^{k+1,k+2}\right) + \frac{2}{15}\left(e^k S_{Q_{\alpha\beta}}^k + e^{k+1} S_{Q_{\alpha\beta}}^{k+1}\right)\tau_\beta^{k,k+1} \tag{2.22}$$

- Interlaminar normal stress:

$$D_z^{k,k+1} - \gamma_z^{k,k+1} = \frac{9}{70}\left(e^k S_v^k v^{k-1,k} + e^{k+1} S_v^{k+1} v^{k+1,k+2}\right) + \frac{13}{35}\left(e^k S_v^k + e^{k+1} S_v^{k+1}\right) v^{k,k+1} \tag{2.23}$$

The three localized interface displacements or slips $\gamma_x^{k,k+1}$, $\gamma_y^{k,k+1}$ and $\gamma_z^{k,k+1}$ can be, for instance, considered as elastic or plastic.

Then, in this approach, two factors may influence the interfacial rigidity between two layers: the rigidity of adjacent layers $\left(S_{Q_{\alpha\beta}}^k, S_v^k, S_{Q_{\alpha\beta}}^{k+1} \text{ and } S_v^{k+1}\right)$ and the own behavior of the interface. The role of a thick or/and inelastic adhesive could be then represented by $\gamma_x^{k,k+1}, \gamma_y^{k,k+1}$ and $\gamma_z^{k,k+1}$. Poor interfacial stiffness or sliding may cause a remarkable decrease of the structure rigidity when a perfect interface (infinite stiffness) provides the expected theoretical and ideal stiffness of the structure. The different interface representations can be summarized as follows in Table 1 with the main governing equations and the application cases.

In this paper, for the study of delaminated beams, a type B description (Table 1) will be considered for interfaces. Type B consider an elastic interface, as if interface can be represented with pure elastic connectors. The three stiffnesses $k_x^{k,k+1}, k_y^{k,k+1}$ and $k_z^{k,k+1}$ in Eqs. (2.24) and (2.25), represent the stiffnesses of such an interface in the different directions (Duong et al., 2011). It has to be noted that due to Eqs. (2.22) and (2.23) which are necessary to calculate localized interface displacements (or slips) $\gamma_x^{k,k+1}$, $\gamma_y^{k,k+1}$ and $\gamma_z^{k,k+1}$, a coupling with adjacent layers is hidden in Eqs. (2.24) and (2.25). This behavior is complex and inherent to the *LS1* model and has not to be seen just as springs relying nodes. However, such solutions exist and give interesting results, for example based on cohesive zone models (for instance in Vandellos et al., 2013) or on direct finite element solutions linking FSDT plates with interface elements (Bruno et al., 2005). For the non-delaminated area, quasi infinite stiffnesses will be used (meaning a behavior similar to a perfect interface of type A) and for the delaminated area, very weak stiffnesses will be used. For pure numerical limitations of *MPFEAP*, a given interface must be described by only one type of interface, the reason why a type A is not used for the non-delaminated area. It has been checked that the arbitrary choices of "infinite" and "weak" values of stiffnesses, represent correctly a respectively perfect and delaminated interface, and permit a convergence of the calculation (see Section 3.2).

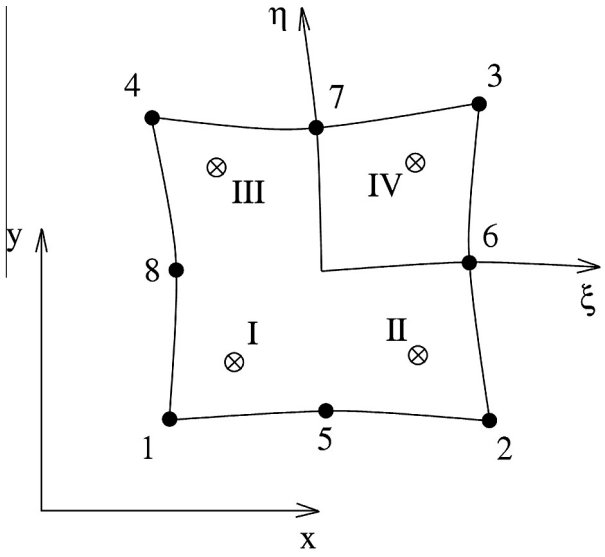

Fig. 2. Element *M4*.

$$\begin{bmatrix}\gamma_x^{k,k+1}\\ \gamma_y^{k,k+1}\end{bmatrix} = \begin{bmatrix}1/k_x^{k,k+1} & 0\\ 0 & 1/k_y^{k,k+1}\end{bmatrix}\begin{bmatrix}\tau_x^{k,k+1}\\ \tau_y^{k,k+1}\end{bmatrix} \tag{2.24}$$

$$\gamma_z^{k,k+1} = \frac{v^{k,k+1}}{k_z^{k,k+1}} \tag{2.25}$$

2.5.2. Numerical formulation with MPFEAP

Based on the previous model *LS1*, as said before, a C^0 finite element model, involving an eight-node isoparametric quadrilateral element with 5n d.o.f at each nodal point and four second-order Gaussian points was formulated. *MPFEAP* permits solution of static and dynamic laminated plate problem with interfaces of type A, B and D. The geometry is meshed with square master elements defined in the ξ, η space. The element is described by eight nodal points and by the shape function $Pk(\xi, \eta)$ (Fig. 2).

3. Application of the *LS1* to delaminated composite beams

In this part, the *LS1* is applied to classical configurations of cracked composite beams. The case study described and studied in Prombut et al. (2006) allows for direct comparisons between 3D FEM, the present approach and experimental results.

Table 1
Type of interfacial behaviors and *LS1* corresponding references.

Type	Denomination	Details and references
A	Elastic composite (*LS1*)	Perfect interface (2.12) and (2.13) Carreira et al. (2002)
B	Elastic composite with elastic interface	Interface with zero thickness and isotropic stiffness (2.24) and (2.25) Duong et al. (2011)
C	Elastic composite with plastic slips	Interface with zero thickness and a perfectly plastic law for interfacial slips Diaz and Caron (2006a)
D	Elastic composite with elastoplastic interface	Interface with non-zero thickness and elastoplastic behavior Duong et al. (2011)

3.1. Case study Prombut et al. (2006)

The following case study is directly derived from Prombut et al. (2006). The main objective of this case study Prombut et al. (2006) was to develop a methodology for establishing crack propagation criteria of unidirectional (UD) and multidirectional (MD) laminates at respectively 0°/0° and 0°/45° interfaces. In this work, the author focused on determining the critical strain energy release rate (SERR) in mode I, G_{Ic} under the conventional double cantilever beam (DCB) (Fig. 3) test method. However, multidirectional delamination interfaces suffer the change of delamination plane under this test configuration Andersons and König (2004). So, the author used the asymmetric double cantilever beam (ADCB) and asymmetric mixed-mode flexure (AMMF) Kinloch et al. (1993) methods to obtain mixed-mode I + II loading with high mode I content in order to determine the G_{Ic} of the 0°/45° interface. In this paper, some of the test configurations will be investigated with the finite element code based on the *LS1* model for calculating strain energy release rates in these delaminated composite beams. The DCB (for pure mode I), ELS (end loaded split for pure mode II) (Fig. 4) MMF (Fig. 5) and ADCB (for mixed-mode I + II) for the 0°/0° interface and the ADCB for the0°/45° one.

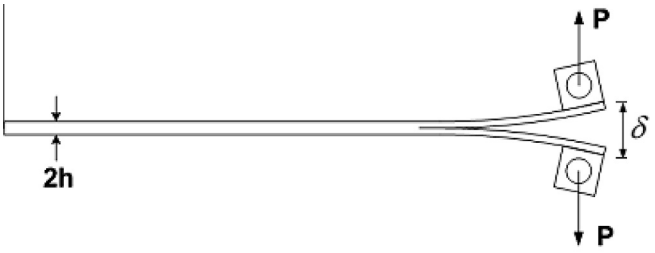

Fig. 3. Double cantilever beam test specimen $(0_6//0_6)$.

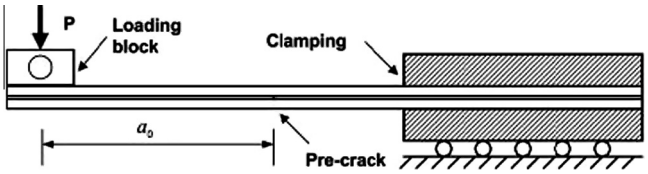

Fig. 4. End loaded split test specimen $(0_9//0_9)$.

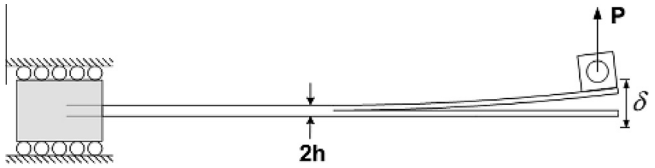

Fig. 5. Mixed mode flexure test specimen $(0_9//0_9)$.

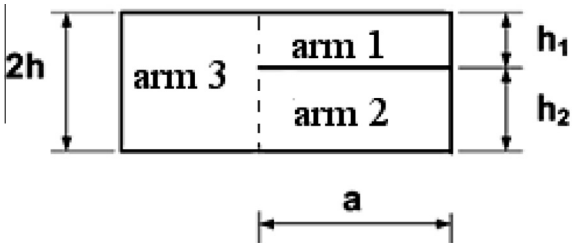

Fig. 6. Sublaminates decomposition of a delaminated beam.

As in Prombut et al. (2006), the stacking sequence for the multidirectional specimens was carefully selected using classical lamination theory (CLT), described by (3.1), in order to eliminate in-plane coupling and in-plane/out-of-plane coupling in each part of the specimen: arm 1 and arm 2 in the cracked region, the uncracked part called arm 3 (Fig. 6). The matrix B of each sublaminate is then a zero matrix. The in-plane extensional/shear coupling must also be eliminated ($A16 = A26 = 0$).

$$\begin{bmatrix} N_1 \\ N_2 \\ N_6 \\ M_1 \\ M_2 \\ M_6 \end{bmatrix} = \begin{bmatrix} A_{11} & A_{12} & A_{16} & B_{11} & B_{12} & B_{16} \\ A_{12} & A_{22} & A_{26} & B_{12} & B_{22} & B_{26} \\ A_{16} & A_{26} & A_{66} & B_{16} & B_{26} & B_{66} \\ B_{11} & B_{12} & B_{16} & D_{11} & D_{12} & D_{16} \\ B_{12} & B_{22} & B_{26} & D_{12} & D_{22} & D_{26} \\ B_{16} & B_{26} & B_{66} & D_{16} & D_{26} & D_{66} \end{bmatrix} \begin{bmatrix} \epsilon_1 \\ \epsilon_2 \\ \epsilon_6 \\ \chi_1 \\ \chi_2 \\ \chi_6 \end{bmatrix} \tag{3.1}$$

In Prombut et al. (2006) the bending/bending and bending/twisting coupling were also minimized: Since the SERR varies across the specimen width, it is desirable to have relatively flat and symmetrically distributed SERR profile. Two non-dimensional parameters, D_c and B_t, are used to assess the SERR distribution. The D_c indicates the curvature due to longitudinal/transverse bending coupling. It is given by (3.2) with $D_c = 0.25$ as an upper bound Davidson et al. (1996).

$$D_c = \frac{D_{12}^2}{D_{11}D_{22}} \tag{3.2}$$

where D_{ij} is a bending stiffness component in the D matrix of the laminate. The B_t is defined in (3.3) (Sun and Zheng, 1996). This parameter indicates the skewness of the crack profile due to bending/twisting coupling of the specimen arms. It is recommended that B_t be kept minimum to minimize the skewness of the SERR profile.

$$B_t = \left|\frac{D_{16}}{D_{11}}\right| \tag{3.3}$$

Studies were also performed in Prombut et al. (2006) to minimize the effects of thermal residual stresses on the toughness.

Taking into account all these considerations, the best stacking sequence for the multidirectional delaminated specimens (ADCB18) was found to be the following, with "//" representing the delaminated interface.

$0/45/-45/-45/45/0//45/0/-45/0/-45/-45/45/45/0/45/0/-45$.

3.2. Numerical data

MPFEAP is then used in this present paper for the delamination case study. All plies are made up of the same carbon-epoxy material (T700/M21) whose mechanical properties are as follows:

$$E_L = 98.62 \text{ GPa}, \quad E_T = E_N = 7.69 \text{ GPa}$$
$$G_{LT} = G_{LN} = 4.75 \text{ GPa}, \quad G_{TN} = 4.75 \text{ GPa}$$
$$v_{LT} = v_{LN} = 0.3, \quad v_{TN} = 0.3, \quad e^i = 0.26 \text{ mm}$$

In order to take into account easily from a numerical point of view the delaminated and non delaminated zones, interfaces of type B from Table 1 are chosen for both zones of the delaminated interface $k, k+1$. Meaning that in (2.24) and (2.25) stiffness was taken isotropic and a zero stiffness interface was put between the plies where delamination occurred arm 1 and arm 2, while a quasi-perfect interface is considered in arm 3 by electing $k_x^{k,k+1} = k_y^{k,k+1} = k_z^{k,k+1} = 3500$ GPa to represent an infinite stiffness. It has been verified that this value is high enough not to influence the results of the finite element simulations as shown in Fig. 7.

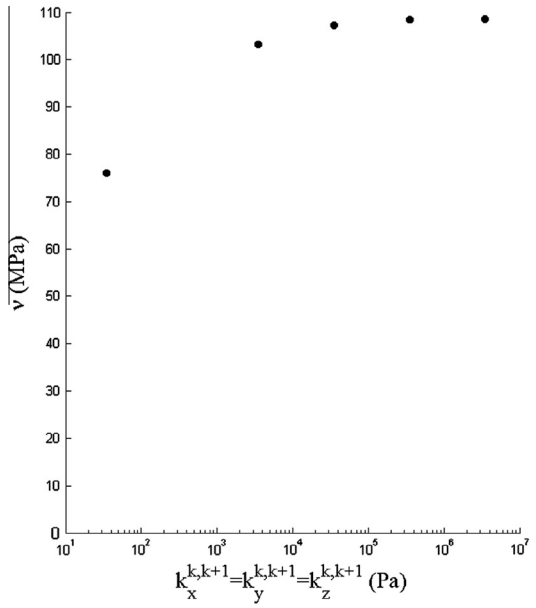

Fig. 7. Normal stress v at delamination front of multidirectional ADCB specimen for different interface stiffnesses.

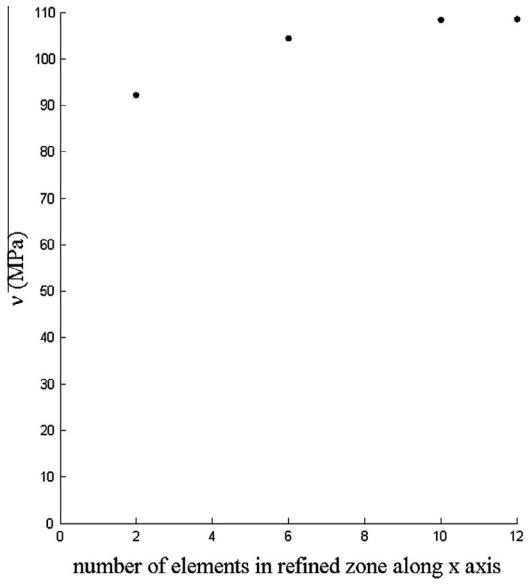

Fig. 9. Normal stress v at delamination front of multidirectional ADCB specimen for different refinements.

It must be highlighted that the *LS1* model permits to measure directly the singularity's stress intensity at delamination front since providing finite stress values. Consequently the finite element approach (with *MPFEAP*) becomes easier since it avoids infinite values due to the 3D singularity and resulting high mesh refinements. The reason of this property is that the integration on a characteristic length often help the designer to obtain a singularity's intensity. Such methods are widely used for stress intensity estimation in composite materials. Characteristic length may be, an arbitrary part of the interface (average stress concept Brewer and Lagace, 1988; Whitney and Nuismer, 1974) or a spherical volume around the singularity (Hochard et al., 2007; Tan, 1988). In this way the *LS1* method has also its characteristic length, the ply thickness, appearing naturally since the 3D fields are integrated along the thickness of the ply. It regulates considerably the stress fields, and provides a kind of "mean" stress value concentrated on the edge, very closed to the concept of stress intensity factor K defined at a crack tip in the linear fracture theory. This remark will be strengthen further in the paper when strain energy release rate (SERR) will be expressed thanks to the *LS*1 model (Section 4.3). Consequently and concerning the meshing, a 5×20 2D-mesh (Fig. 8) with a refinement in the vicinity of the delamination front (up to 5 mm from the crack tip along x axis in the non-delaminated zone) was enough to obtain the convergence of the interfacial stresses of the *LS1* model at delamination front. These interfacial stresses reach a plateau when the number of elements in the refined zone along x axis is equal to 10 as it is shown in Fig. 9.

In order to evaluate the model performance on delaminated composite beams for structural analysis, 12-layers unidirectional DCB and ADCB tests and 18-layers multidirectional ADCB test described in the previous paragraph were investigated and the displacements results of the *LS1* model for different crack lengths were compared to those of a 3D finite element model from Prombut et al. (2006). To illustrate the results obtained for the ADCB test specimen with *MPFEAP*, and since the deformed global 2D model remains naturally quite flat even in the delaminated region (a same physical node cannot move uphill and downhill in the same time), the top and bottom layers deflections were post-processed, considering a delamination length $a = 95$ mm, and represented in Fig. 10. The specimen is clamped at one end by blocking displacements and rotations of the nodes at the border. The loading is applied in the z direction at the other end by distributing the load P on the nodes at the border for the top layer and $-P$ for the bottom layer. The strain energy release rates determination will be treated in Section 4.

3.3. Displacements/crack length results

The results of each test configuration were obtained by averaging the experimental critical forces and displacements corresponding to different measured crack length in Prombut et al. (2006). Tables 2 and 3 results reports the average experimental load, P, and displacement values $\delta - EXP$ obtained for each crack length, as well as the displacements obtained from the finite element models both from Prombut et al. (2006) and from *MPFEAP* named respectively $\delta - 3DFE$ and $\delta - MPFEAP$ for different test configurations. The correlation between the 3D finite elements and the *LS1* model is reasonably good. The average displacement difference between experimental and *MPFEAP* values is $< 7\%$ for the worst case with a really light and 2D mesh.

Fig. 8. Typical 2D-mesh of a test specimen.

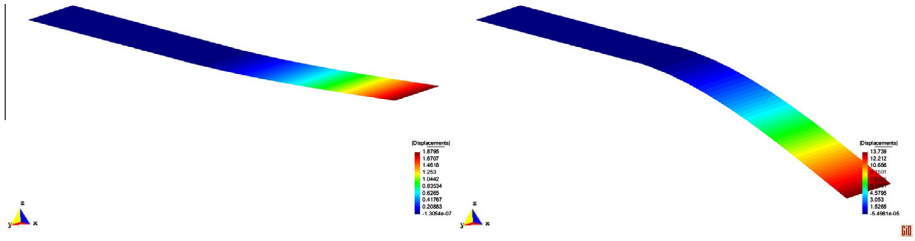

Fig. 10. Deformed model and displacements values of top and bottom layers for unidirectional ADCB delaminated specimen.

Table 2
Simulated and experimental displacements for different crack lengths of unidirectional DCB and ADCB specimens.

DCB	a(mm)/P(N)	45/51.19	50/49.63	55/47.61	60/46.27	65/45.11
	δ-EXP (mm)	5.76	7.41	9.35	11.16	13.31
	δ-3DFE (mm)	5.58	7.27	9.12	11.33	13.85
	δ-MPFEAP (mm)	5.32	6.93	8.72	10.84	13.31
ADCB	a(mm)/P(N)	45/41.98	50/40.75	55/40.73	60/39.72	65/37.20
	δ-EXP (mm)	8.06	10.35	13.01	16.02	19.01
	δ-3DFE (mm)	8.07	10.53	13.72	17.06	20.07
	δ-MPFEAP (mm)	7.98	10.11	12.82	15.78	18.99

Table 3
Simulated and experimental displacements for different crack lengths of multidirectional ADCB specimen.

ADCB18	a(mm)/P(N)	85/26.21	90/25.17	95/24.82	100/24.28	105/22.83
	δ-EXP (mm)	15.01	16.93	19.32	22.37	23.87
	δ-3DFE (mm)	13.23	14.98	17.24	19.54	21.19
	δ-MPFEAP (mm)	12.63	14.31	16.51	18.75	20.33

4. Different methods for strain energy release rate and mode ratio determination

The strain energy release rate G can be calculated by different methods on tests specimens. Those methods are based on the main definition of G

$$G = -\frac{\partial \Pi}{\partial A} \tag{4.1}$$

where A is the delaminated area. Recall that the total elastic potential energy, Π is given by the inner force system potential, U, and the external force potential, Ω.

$$\Pi = U + \Omega \tag{4.2}$$

where the internal potential is the stored elastic energy, i.e. the strain energy

$$U = \int_V \frac{1}{2}\sigma_{ij}\epsilon_{ij}dV \tag{4.3}$$

According to the definition of G (4.1) we may estimate it by considering a finite crack growth δa, thus a crack extension of the initial crack a, to obtain

$$G \simeq -\frac{\Pi(a+\delta a) - \Pi(a)}{\Delta A} = -\frac{\Pi(a+\delta a) - \Pi(a)}{w\delta a} \tag{4.4}$$

where w is the width of the component.

In the following paragraphs, the different strain energy release rates calculation methods will be presented: experimental determination, numerical calculation and formulation derived from the *LS1* model.

4.1. Experimental determination

For the experimental determination of strain energy release rate, data reduction was based on beam theory Williams (1989)and compliance method Davies et al. (2001). For mixed-mode loadings it is interesting to identify in the total SERR the part due to mode I G_I and the one due to mode II G_{II}. This mode decomposition was covered with a global approach using modified beam theory for symmetric specimens. For asymmetric specimens, a local approach using the stress intensity factor is requested to obtain the mode ratio Ducept et al. (1999).

4.1.1. Mode I: DCB test

A load P is applied to each arm of a specimen with a delamination length a as in Fig. 3. The deflection of the specimen is measured by the displacement of the crosshead δ. The SERR for mode I, G_I is calculated using the modified beam theory as in Williams (1989):

$$G_I = \frac{3P\delta}{2w(a+\chi h)} \tag{4.5}$$

where h is the thickness of the specimen arm, w its width, and χ a correction factor for the beam section rotation.

4.1.2. Mode II: ELS test

The specimen is clamped in a support that can slide in the longitudinal direction as in Fig. 4. The SERR for mode II, G_{II} is determined from the compliance method on experimental values as in Davies et al. (2001):

$$G_{II} = \frac{3mP^2a^2}{2w} \tag{4.6}$$

where m is the slope of the compliance ($C = \delta/P$) versus a^3.

4.1.3. Mixed mode I/II for symmetric specimen: MMF test

The MMF uses the same fixture as the ELS except that only one arm of the specimen is loaded with the force P, while the other one is free. The G_I and G_{II} are determined from the modified beam theory as in Kinloch et al. (1993):

$$G_I = \frac{6P^2(a+\chi_I h_2)^2}{w^2 E_{1f}} \frac{h_1^3}{h_2^3(h_1^3+h_2^3)}$$
$$G_{II} = \frac{18P^2(a+\chi_{II} h_1)^2}{w^2 E_{1f}} \frac{h_1 h_2}{(h_1+h_2)^2(h_1^3+h_2^3)} \tag{4.7}$$

where h_1 and h_2 are the thicknesses of respectively the free arm and the loaded one, w the width of the specimen and χ_I and $\chi_I I$ are correction factors for the beam section rotation.

4.1.4. Mixed mode I/II for asymmetric specimens: ADCB test

For symmetric specimens, modified beam theory and compliance method also called global method provide good results. However, for non-symmetric specimens Ducept et al. (1999) have shown that another approach was needed. This approach is based on the calculation of stress intensity factors and also called local method. The strain energy release rates in each mode are then deduced using the Irwin relations.

4.2. Numerical methods

Finite elements simulations were performed in Prombut et al. (2006) using both virtual crack extension (VCE) and virtual crack closure technique (VCCT) method as a basis of comparison.

The virtual crack extension (VCE) method was classically used in the finite element models to determine SERR and mode ratio values, the node at the crack front is split into two nodes and each node is moved by a chosen distance. The total SERR is calculated using the change of potential energy in the surrounding elements when considering a variation of crack length due to these virtual nodal displacements, thus needing two finite element calculation.

Mode ratio is then determined using nodal forces and opening displacements components of these split nodes.

The virtual crack closure technique (VCCT) is based on the assumption that the energy needed to separate a surface when a crack grows δa, is the same energy needed to close the same surface δa.

It is further assumed that the crack grows in a self-similar manner, such that the stress states around the crack tip do not change significantly when the crack grows a small amount δa.

This means in the nearby of a crack, from one crack step to another, it is expected to see the same crack shape, the same displacements, and about the same forces.

With this simplification it is possible to use the same finite element simulation to extract reaction forces and displacements required to close the crack δa, thereby reducing the computational efforts.

The strain energy release rate can be estimated by:

$$G = G_I + G_{II} \simeq \frac{1}{2}\frac{F_x \delta u}{\delta a w} + \frac{1}{2}\frac{F_y \delta v}{\delta a w} \tag{4.8}$$

where $\delta u = u - u'$ and $\delta v = v - v'$ as defined in Fig. 11.

Finite elements simulations were performed in Prombut et al. (2006) using both virtual crack extension and virtual crack closure technique method as a basis of comparison.

4.3. LS1 formulation Diaz et al. (2007) with VCCT method

The SERR and mode partitioning can be calculated efficiently by using the *LS1* model and the VCCT method. Indeed, SERR of a given mode, appears as a function of the interfacial stresses of the model at the delaminated interface $\tau_x^{k,k+1}, \tau_y^{k,k+1}$ or $\nu^{k,k+1}$ and of specific Ψ functions which depend only on the stacking sequence and z-position of delamination, as it will be shown hereafter. In particular, Ψ functions do not depend on the loading, the plate global geometry or the crack length. This method is of great interest as it allows on simple cases pure analytical determination of the SERR mode ratio (Diaz et al., 2007; Saeedi et al., 2012a). In the present paper it will be shown that for more complex structures, SERR determination needs only interfacial stresses calculation with *MPFEAP* simulation while the Ψ functions are analytically calculated, once, even if the delamination propagates or the prescribed loading is modified.

When VCCT method is applied using the *LS1* interfacial stresses $\tau_x^{k,k+1}, \tau_y^{k,k+1}$ and $\nu^{k,k+1}$ (defined in Eqs. (2.4) and (2.5)) and local interface displacements (slips) $\gamma_x^{k,k+1}, \gamma_y^{k,k+1}$ and $\gamma_z^{k,k+1}$ (formulated in paragraph 2.5.1) at the delaminated interface $k, k+1$, the following relations for the strain energy release rates in the different modes G_I, G_{II} and G_{III} are obtained and proposed firstly in Diaz et al. (2007):

$$G_I = \frac{1}{2}\nu^{k,k+1}\gamma_z^{k,k+1} \tag{4.9}$$

$$G_{II} = \frac{1}{2}\tau_x^{k,k+1}\gamma_x^{k,k+1} \tag{4.10}$$

$$G_{III} = \frac{1}{2}\tau_y^{k,k+1}\gamma_y^{k,k+1} \tag{4.11}$$

By expressing interfacial slips $\gamma_x^{k,k+1}, \gamma_y^{k,k+1}$ and $\gamma_z^{k,k+1}$ with respect to interfacial stresses $\tau_x^{k,k+1}, \tau_y^{k,k+1}$ and $\nu^{k,k+1}$ the relations between strain energy release rates and interfacial stresses at crack front are obtained (see details in A.2). These relations involve five ψ functions $\psi^{\nu}, \psi_{xx}^{\tau}, \psi_{xy}^{\tau}, \psi_{yy}^{\tau}$ and ψ_{yx}^{τ} depending only of the stacking sequence and the position of the delamination (Diaz et al., 2007):

$$G_I = \psi^{\nu}(\nu^{k,k+1})^2 \tag{4.12}$$

$$G_{II} = \psi_{xx}^{\tau}(\tau_x^{k,k+1})^2 + \psi_{xy}^{\tau}\tau_y^{k,k+1}\tau_x^{k,k+1} \tag{4.13}$$

$$G_{III} = \psi_{yy}^{\tau}(\tau_y^{k,k+1})^2 + \psi_{yx}^{\tau}\tau_x^{k,k+1}\tau_y^{k,k+1} \tag{4.14}$$

These relations, (4.12)–(4.14) are general and for any cracked laminate. For multi-cracked laminates they are also relevant after a virtual cutting of the specimen in zones with different number of delaminations to calculate the corresponding ψ functions. The different strain energy release rates are then expressed as squared form of interfacial stresses $\tau_x^{k,k+1}, \tau_y^{k,k+1}$ and $\nu^{k,k+1}$ multiplied by functions of the elastic properties of the test specimen $\psi^{\nu}, \psi_{xx}^{\tau}, \psi_{xy}^{\tau}, \psi_{yy}^{\tau}$ and ψ_{yx}^{τ}.

It has to be noted that there are some similarities between expressions (4.12)–(4.14) and the strain energy release rate

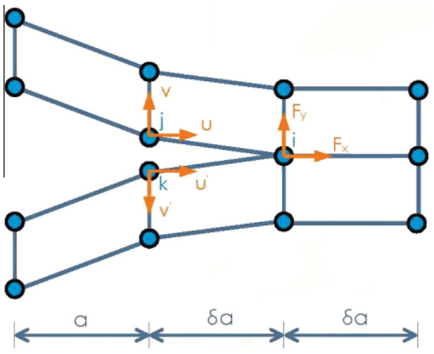

Fig. 11. Finite element model using VCCT method (crack length $a + \delta a$).

expressed in terms of stress intensity factors K as showed by Irwin (1957), where for example G_I calculated under plain strain assumption for an isotropic material is given by:

$$G_I = \frac{1-\nu^2}{E} K_I^2 \tag{4.15}$$

The *LS1* interfacial shear, $\tau_x^{k,k+1}$ and $\tau_y^{k,k+1}$, and normal stress $\nu^{k,k+1}$ in (4.12)–(4.14), which as said before have a finite value even at free edges or crack tips due to the ply thickness integration process present some similarities with the stress intensity factors K, and appear then as a relevant tool for the measurement of the stress intensity at delamination front.

5. Application to case study

These different methods for calculation of SERR and mode partitioning were compared on DCB, ELS, MMF and ADCB unidirectional test specimens and on ADCB18 multidirectional one from Prombut et al. (2006).

In Prombut et al. (2006) is also proposed the calculation of these critical strain energy release rate by classical three-dimensional (x, y, z) finite element models using crack lengths and their corresponding critical forces from the experimental data. Invariance in the y direction is assumed and the geometrical description becomes two-dimensional (x-z plane), even if it remains basically for us a 3D approach since a through the thickness (z) description of the fields is necessary. In the following these results are referenced as *G-3DFE*. The models were created with 8-node elements under a plane strain assumption. Each ply was modeled individually along the thickness. The longitudinal mesh was refined at around the crack tip so that the element size was the one of a ply (Fig. 12).

Concerning the *MPFEAP* model, the same mesh and delaminated interface creation as in Section 3.2 and on Fig. 8 was used in GiD to obtain the values of the interfacial stresses $\tau_x^{k,k+1}$, $\tau_y^{k,k+1}$ and $\nu^{k,k+1}$ of the *LS1* model. Thus, the critical strain energy release rates corresponding to experimental measures will be determined using Eqs. (4.12)–(4.14), and the ψ functions calculated as in the next section. In the following *MPFEAP* results for G are referenced as *G-MPFEAP* and correspond to the values obtained at the mid-point of the delamination front in the y-direction, which are the most coherent for a comparison with results arising from plane strain assumption.

5.1. Calculation of ψ functions

As previously mentioned with *LS1* model, it is possible to calculate directly the strain energy release rates for each mode as in (4.12)–(4.14), using the same ψ functions no matter the crack length or loading conditions as they depend only on the stacking sequence and the position of the delaminated interface.

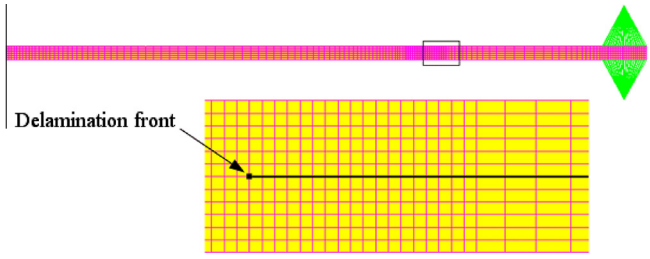

Fig. 12. Finite element model under plane strain assumption of Prombut et al. (2006).

These functions can be calculated analytically using the stiffness and thickness parameters of each layer and its position in the stacking sequence. For example in the case of a bilayer DCB specimen (see A.3):

$$\psi^{\nu} = \frac{13}{35}\left(e^1 S_{\nu}^1 + e^2 S_{\nu}^2\right) \tag{5.1}$$

where e^1 and e^2 are the thicknesses of each layer, S_{ν}^1 and S_{ν}^2 their normal compliances (S_{zzzz}^i component of the 3D compliance S^i of layer i).

For more complex situations, ψ functions can be also analytically calculate by inverting a system as in A.2. Here, ψ^{ν} and ψ_{xx}^{τ} (the only functions involved in the following study as $\tau_y^{k,k+1} = 0$) were calculated for an 18-layers unidirectional specimen and were used to calculate strain energy release rates in respectively double cantilever beam ($DCB18U_{85}$) and end load split ($ELS18U_{85}$) test configuration with a delamination length of 85 mm.

These elementary calculations were made using Eqs. (4.12) and (4.13) with the interfacial stresses $\tau_x^{k,k+1}$ and $\nu^{k,k+1}$ found numerically with MPFEAP.

The strain energy release rates G_I and G_{II} were then compared with the ones found experimentally and calculated with finite elements by Prombut et al. (2006) as reported in Table 4. The good correlation between the experimental SERR and the *LS1* model despite the light mesh and direct calculation of the SERR shows the efficiency of this approach.

5.2. The functions ψ are independent of the loading case

To validate the fact that these functions are independent of loading cases but depend only of material and stacking sequence, the previously calculated values of ψ^{ν} and ψ_{xx}^{τ} were then used in Eqs. (4.12) and (4.13) to calculate the strain energy release rates in mode I and mode II of another case loading of the same 18-layers unidirectional sequence, a mixed-mode flexure ($MMF18U_{85}$) specimen with same geometry as $DCB18U_{85}$ and $ELS18U_{85}$. The interfacial stresses $\tau_x^{k,k+1}$ and $\nu^{k,k+1}$ were calculated with MPFEAP under the experimental load given in Prombut et al. (2006).

Table 5 results report the average experimental SERR values and mode partitioning for the $MMF18U_{85}$ test, as well as those obtained from the finite element models both from Prombut et al. (2006) and from MPFEAP named respectively $G-3DFE$ and $G-MPFEAP$. The correlation between experimental SERR and the *LS1* model is a bit better than the 3D finite elements.

Then, for a given stacking sequence, the *LS1* model allows for direct calculation of strain energy release rates under various loadings with only one determination of the different ψ functions.

Table 4
Average experimental compared to finite element SERR values for $DCB18U_{85}$ and $ELS18U_{85}$ test configurations.

	Method	$G-EXP$	$G-3DFE$	$G-MPFEAP$
$DCB18U_{85}$	G_I (J/m^2)	392	421	409
$ELS18U_{85}$	G_{II} (J/m^2)	1211	1141	1176

Table 5
Average experimental compared to finite element SERR values for $MMF18U_{85}$ test configuration, with same ψ^{ν} and ψ_{xx}^{τ} as used on $DCB18U_{85}$ and $ELS18U_{85}$.

$MMF18U_{85}$	Method	$G-EXP$	$G-3DFE$	$G-MPFEAP$
	G_I (J/m^2)	385	547	340
	G_{II} (J/m^2)	290	277	329

Table 6
Average experimental compared to finite element SERR values for DCB test configuration.

DCB	a(mm)/P(N)	45/51.19	50/49.63	55/47.61	60/46.27	65/45.11
	$G_I - EXP\ (J/m^2)$	426	479	527	560	602
	$G_I - 3DFE\ (J/m^2)$	451	515	567	629	694
	$G_I - MPFEAP\ (J/m^2)$	436	494	539	593	645

Table 7
Average experimental compared to finite element SERR values for ADCB18 unidirectional test configuration.

ADCB18	a(mm)/P(N)	85/34.17	90/31.93	95/31.31	100/29.56	105/28.73
	$G_I - EXP\ (J/m^2)$	321	314	337	332	346
	$G_I - 3DFE\ (J/m^2)$	327	319	340	335	347
	$G_I - MPFEAP\ (J/m^2)$	315	304	325	322	335
	$G_{II} - EXP\ (J/m^2)$	59	58	62	61.5	64
	$G_{II} - 3DFE\ (J/m^2)$	46	45	48	47	49
	$G_{II} - MPFEAP\ (J/m^2)$	70	68	73	72	75

Table 8
Finite element SERR values for ADCB18 multidirectional test configuration.

ADCB18	a(mm)/P(N)	85/26.21	90/25.17	95/24.82	100/24.28	105/22.83
	$G_I - 3DFE\ (J/m^2)$	272	280	301	318	309
	$G_I - MPFEAP\ (J/m^2)$	273	280	303	320	311
	$G_{II} - 3DFE\ (J/m^2)$	16	16	17	18	17
	$G_{II} - MPFEAP\ (J/m^2)$	15	15	16	18	16

5.3. Calculation of SERR for different delamination length in DCB and ADCB

Using the same test configuration as in paragraph 3.2, it was possible to calculate the ψ functions in (4.12) and (4.13) as explained in paragraph 5.1 and calculate the strain energy release rates for an initial delamination length $a_0 = 45$ mm for the DCB specimen and $a_0 = 85$ mm for the ADCB unidirectional and multidirectional ones.

In these cases, the position of delamination and the number and orientation of layers were different from the tests used in Sections 5.1 and 5.2, thus the need of a new calculation of ψ^v for DCB specimen and ψ^v and ψ^{τ}_{xx} for the ADCB one.

Other values of SERR for longer delamination of same specimens were then calculated using the same ψ functions, calculated for the initial delamination length, and the different interfacial stresses results corresponding to different crack length given by MPFEAP.

Tables 6–8 results report the average experimental SERR values and mode partitioning, as well as those obtained from the finite element models both from Prombut et al. (2006) and from MPFEAP named respectively $G - 3DFE$ and $G - MPFEAP$. The correlation between the 3D finite elements and the *LS1* model is reasonably good.

6. Conclusion

The delamination phenomenon is one of the major issues in design of multilayer structures. In order to apply a delamination failure criterion, it is necessary, to analyze the delaminated structure and above all, to identify a relevant measure of phenomena. Since 3D finite element models are generally too expensive in terms of computational time and memory for such analysis, many researches are dedicated to approach delamination problems with alternative methods such as 2D layerwise models. The proposed method is based on the formulation of the *LS1* model (Caron et al., 2006) which is a layerwise stress approach with first-order membrane stress approximation per layer. The model can be described as a stacking sequence of Reissner–Mindlin plates linked by interlaminar stresses. This model was already used and validated for analyzing multilayered plates under various loadings in non-delaminated state (Carreira et al., 2002) and some analytical developments were made to take into account delamination in mode III at free edges under uniaxial extension (Diaz et al., 2007; Saeedi et al., 2012a).

In the present work, the *LS1* model was applied to the analytical and numerical analysis of delamination propagation in multilayered specimens subjected to classical loads in Mode I and/or Mode II.

In order to test the numerical formulation based on the *LS1* for delamination propagation analyzes, strain energy release rates comparisons were made between the *LS1* model and a 3D-FEM from Prombut et al. (2006) for different test specimens such as DCB for pure mode I, ELS for pure mode II and ADCB for mixed-mode I/II and two different delaminated interfaces 0°/0° and 0°/45°. The delaminated and non-delaminated interfaces were represented numerically by respectively a zero and a quasi-infinite stiffness. It has been shown that the strain energy release rate values determined using interfacial stresses and Ψ functions from the *LS1* model are in really good agreement with experimentation and 3D-FEM proposed in Prombut et al. (2006), which is remarkable given the very direct and light method used in this paper. The interesting property is that only one calculation of the different ψ functions, linking interfacial stresses and the strain energy release rates in both modes G_I and G_{II}, is needed for a stacking sequence and a position of delamination, no matter the loading nor the length of the delamination. Thus, it will be possible to calculate really complex delaminated structures, and predict delamination using a specific delamination criterion. These criteria are usually presented in the form of an analytic expression that

interpolates between the pure mode I, mode II and mode III loadings and fracture toughness. Among the different failure criteria to predict delamination propagation under mixed-mode loading available in the literature, the Power Law criterion Wu and Reuter, 1965 and Benzeggagh and Kenane (B&K) (1996) criterion could be used along with results from the *LS1* model. These energy criteria would become interfacial stress based ones using the relations involving the ψ functions and thus would be of direct use to predict delamination propagation.

The main advantage of using this model is that it needs only one 2D plate FE calculation with low mesh refinement, reducing drastically computational time. If there exist several delaminated interfaces, it does not really affect neither the description nor the calculation. It remains a plate description in the plane x-y. For a classical 3D finite element approach it leads to a really new meshing, to refinements close to the new delaminations, and in the adjacent layers. Moreover, elements have to be well conditioned and respect relevant slenderness: increasing the refinement through the thickness, leads to increase the refinement in the x-y plane. At last, an *MPFEAP* element possesses only 4 Gauss points through the entire thickness, when 8 Gauss points for each 3D element of the z-refinement are necessary. The number of dof and time calculation increase necessarily very quickly. We do not quantify the gap for these specific examples, as we did not carry out the 3D FE calculations ourself but used those of Prombut et al. (2006). However, we did it in Duong et al. (2011) and the method proves to be obviously and *fundamentally* lighter. Finally, despite this lightness, the comparisons between the *LS1* model and the 3D-FEM regarding strain energy release rates and displacements, clearly show the usefulness and efficiency of the *LS1* model as a layerwise stress model for delamination analysis of complex and huge structures, and for criteria proposals. This latter point is in progress.

Appendix A

A.1. Introduction

In order to express interfacial slips $\gamma_x^{k,k+1}$, $\gamma_y^{k,k+1}$ and $\gamma_z^{k,k+1}$ with respect to interfacial stresses $\tau_x^{k,k+1}$, $\tau_y^{k,k+1}$ and $\nu^{k,k+1}$, the following equation manipulations are necessary.

- By taking the difference of the *LS1* interfacial behavior Eqs. (2.22) and (2.23), both in delaminated zone and non-delaminated one,
- Then by using the continuity of the generalized displacements $D_\alpha^{i,i+1}$ and $D_z^{i,i+1}$, as a consequence of their definition in (2.12) and (2.13),
- And the continuity of Φ_α, U_α and U_z in layers i and $i+1$, and of the shear forces Q_x^i and Q_x^{i+1} defined in (2.3),

relations between slips and interfacial stresses are obtained.

However, these equations for the in-plane slips are also written with respect to shear forces differences ΔQ_y^i and ΔQ_y^{i+1}. Taking the difference of shear force behavior Eq. (2.16) in delaminated and non-delaminated zone gives these shear forces variations with respect to interfacial stresses variations at interface $i-1/i, i/i+1$ and $i+1/i+2$. Taking all these equations under matrix form it will be possible to write the system as secondary unknowns $\gamma_x^{k,k+1}, \gamma_y^{k,k+1}$ and $\gamma_z^{k,k+1}$ with respect to primary unknowns $\tau_x^{k,k+1}, \tau_y^{k,k+1}$ and $\nu^{k,k+1}$ as shown hereafter.

A.2. Determination of the in-plane slips $\gamma_x^{k,k+1}$ and $\gamma_y^{k,k+1}$

In the appendix introduction was explained how to obtain a system of $3n-2$ equations which can be expressed under the following matrix form:

$$\tilde{\tilde{\Lambda}}^1 \tilde{\chi}^1 = -\tilde{\gamma} \tag{A.1}$$

where $\tilde{\chi}^1$ is a $3n-2$ dimension vector defined by

$$\tilde{\chi}^{1t} = \left[\Delta Q_1^1, \ldots, \Delta Q_1^n, \Delta\tau_1^{1,2}, \ldots, \Delta\tau_1^{n-1,n}, \Delta\tau_2^{1,2}, \ldots, \Delta\tau_2^{n-1,n}\right] \tag{A.2}$$

and $\tilde{\gamma}$ is a $3n-2$ dimension vector defined by

$$\tilde{\gamma}^t = \left[\underbrace{0,..,0}_{n+k-1}, \gamma_x^{k,k+1}, \underbrace{0,..,0}_{n-2}, \gamma_y^{k,k+1}, \underbrace{0,..,0}_{n-k-1}\right] \tag{A.3}$$

$\tilde{\tilde{\Lambda}}^1 = (\lambda_{pq})_{1\leqslant p,q\leqslant 3n-2}$ is the following $(3n-2)X(3n-2)$ dimension matrix

$$\tilde{\tilde{\Lambda}}^1 = \begin{bmatrix} \tilde{\tilde{C}}_1 & \tilde{\tilde{A}}_{11}^t & \tilde{\tilde{A}}_{12}^t \\ \tilde{\tilde{A}}_{11} & \tilde{\tilde{D}}_{11} & \tilde{\tilde{D}}_{12} \\ \tilde{\tilde{A}}_{12} & \tilde{\tilde{D}}_{12} & \tilde{\tilde{D}}_{22} \end{bmatrix} \tag{A.4}$$

$\tilde{\tilde{A}}_{ij}$ is a $(n-1)Xn$ dimension matrix defined for $(i,j)\in\{1,2\}^2$ by

$$\tilde{\tilde{A}}_{ij} = -\frac{1}{10}\begin{bmatrix} S_{Qij}^1 & S_{Qij}^2 & 0 & & 0 \\ 0 & S_{Qij}^2 & S_{Qij}^3 & & 0 \\ & & \cdot & \cdot & \\ & & & \cdot & \cdot \\ 0 & & & S_{Qij}^{n-1} & S_{Qij}^n \end{bmatrix} \tag{A.5}$$

$\tilde{\tilde{C}}_i$ is a $(n-1)Xn$ dimension matrix defined for $i\in\{1,2\}$ by

$$\tilde{\tilde{A}}_{ij} = \frac{6}{5}\begin{bmatrix} \frac{S_{Q1i}^1}{e^1} & 0 & & 0 \\ 0 & \frac{S_{Q1i}^2}{e^2} & & 0 \\ & & \cdot & \\ & & & \cdot \\ 0 & 0 & & \frac{S_{Q1i}^n}{e^n} \end{bmatrix} \tag{A.6}$$

and $\tilde{\tilde{D}}_{ij}$ a $(n-1)X(n-1)$ dimension matrix defined for $(i,j)\in\{1,2\}^2$ by

$$\tilde{\tilde{D}}_{ij} = \begin{cases} \frac{1}{30}\left(4\left(e^1 S_{Qij}^1 + e^2 S_{Qij}^2\right)\right) & \text{if } n=2 \\ \frac{1}{30}\left(4\left(e^p S_{Qij}^p + e^{p+1} S_{Qij}^{p+1}\right)\delta_{p,q} - e^p S_{Qij}^p \delta_{p,q+1} - e^q S_{Qij}^q \delta_{p+1,q}\right) & \text{if } n\geqslant 3 \end{cases} \tag{A.7}$$

with $\delta_{i,j}$ the Kronecker symbol.

Let's consider the following submatrices of the matrix $\tilde{\tilde{\Lambda}}^1$:

- $\tilde{\tilde{\Lambda}}^2$ a $(3n-4)X(3n-4)$ dimension matrix obtained from $\tilde{\tilde{\Lambda}}^1$ by removing lines and columns $n_1=(n+k)$ and $n_2=(2n-1+k)$.
- $\tilde{\tilde{\Lambda}}^3$ a $(3n-4)X2$ dimension matrix obtained by removing from columns n_1 and n_2 of $\tilde{\tilde{\Lambda}}^1$ the lines n_1 and n_2.
- $\tilde{\tilde{\Lambda}}^4$ a $2X(3n-4)$ dimension matrix obtained by removing from lines n_1 and n_2 of $\tilde{\tilde{\Lambda}}^1$ the columns n_1 and n_2.
- $\tilde{\tilde{\Lambda}}^5$ a $2X2$ dimension matrix obtained from $\tilde{\tilde{\Lambda}}^1$:

$$\tilde{\tilde{\Lambda}}^5 = \begin{bmatrix} \lambda_{n_1,n_1} & \lambda_{n_1,n_2} \\ \lambda_{n_2,n_1} & \lambda_{n_2,n_2} \end{bmatrix} \tag{A.8}$$

- $\tilde{\chi}^2$ a $(3n-4)$ dimension vector obtained from $\tilde{\chi}^1$ by removing lines n_1 and n_2, representing the secondary unknowns without the displacements discontinuities.
- $\tilde{\chi}^3$ a 2 dimension vector obtained from $\tilde{\chi}^1$ representing the opposite of the main unknowns:

$$\tilde{\chi}^3 = \begin{bmatrix} \chi_{n_1} \\ \chi_{n_2} \end{bmatrix} \tag{A.9}$$

With all the above definitions, the following relation describing the equations not involving the slips $\gamma_x^{k,k+1}$ and $\gamma_y^{k,k+1}$ is obtained:

$$\tilde{\tilde{\Lambda}}^2.\tilde{\chi}^2 = -\tilde{\tilde{\Lambda}}^3.\tilde{\chi}^3 \tag{A.10}$$

which can be written

$$\tilde{\chi}^2 = -\left(\tilde{\tilde{\Lambda}}^2\right)^{-1}.\tilde{\tilde{\Lambda}}^3.\tilde{\chi}^3 \tag{A.11}$$

In the appendix introduction was also obtained for $j = k$ the following family of equations:

$$\tilde{\tilde{\Lambda}}^4.\tilde{\chi}^2 + \tilde{\tilde{\Lambda}}^5.\tilde{\chi}^3 = -\begin{bmatrix}\gamma_x^{k,k+1}\\ \gamma_y^{k,k+1}\end{bmatrix} \tag{A.12}$$

According to (A.11) and by defining:

$$\tilde{\tilde{\Psi}} = -\tilde{\tilde{\Lambda}}^4.\left(\left(\tilde{\tilde{\Lambda}}^2\right)^{-1}.\tilde{\tilde{\Lambda}}^3\right) + \tilde{\tilde{\Lambda}}^5 \tag{A.13}$$

and replacing $\tilde{\chi}^3$ by its expression, the aimed relation is obtained:

$$\begin{bmatrix}\gamma_x^{k,k+1}\\ \gamma_y^{k,k+1}\end{bmatrix} = \tilde{\tilde{\Psi}}.\begin{bmatrix}\tau_x^{k,k+1}\\ \tau_y^{k,k+1}\end{bmatrix} \tag{A.14}$$

A.3. Determination of the out-of-plane slip $v^{k,k+1}$

In the appendix introduction was explained how to obtain a system of n equations which can be expressed under the following matrix form for $n \geqslant 3$:

$$\tilde{\tilde{\kappa}}^1\tilde{v}^1 = -\tilde{\gamma}_z \tag{A.15}$$

where $\tilde{v}^1$ is a $n-1$ dimension vector defined by

$$\tilde{v}^{1t} = \left[\Delta v^{1,2}, \ldots, \Delta v^{n-1,n}\right] \tag{A.16}$$

and $\tilde{\gamma}_z$ is a $n-1$ dimension vector defined by

$$\tilde{\gamma}^t = \left[\underbrace{0,..,0}_{k-1}, \gamma_z^{k,k+1}, \underbrace{0,..,0}_{n-k-1}\right] \tag{A.17}$$

$\tilde{\tilde{\kappa}}^1 = (\kappa_{pq})_{1\leqslant p,q\leqslant n-1}$ is the following $(n-1)X(n-1)$ dimension matrix

$$\tilde{\tilde{\kappa}}^1 = \frac{1}{70}\begin{bmatrix} 26\left(e^1S_v^1 + e^2S_v^2\right) & 9e^2S_v^2 & . & . & . & 0\\ 9e^2S_v^2 & . & . & . & . & 0\\ . & . & . & . & . & .\\ . & . & . & . & . & .\\ 0 & 0 & . & . & . & 9e^{n-1}S_v^{n-1}\\ 0 & 0 & . & . & 9e^{n-1}S_v^{n-1} & 26\left(e^{n-1}S_v^{n-1} + e^nS_v^n\right)\end{bmatrix} \tag{A.18}$$

Let's consider the following submatrices of the matrix $\tilde{\tilde{\kappa}}^1$ for $n \geqslant 3$:

- $\tilde{\tilde{\kappa}}^2$ a $(n-2)X(n-2)$ dimension matrix obtained from $\tilde{\tilde{\Lambda}}^1$ by removing line and column k.
- $\tilde{\kappa}^3$ a $n-2$ dimension vector obtained by removing from column k of $\tilde{\tilde{\kappa}}^1$ the line k.
- $\tilde{\kappa}^4$ a $n-2$ dimension vector obtained by removing from line k of $\tilde{\tilde{\kappa}}^1$ the column k.
- $\tilde{v}^2$ a $(n-2)$ dimension vector obtained from $\tilde{v}^1$ by removing line k, representing the secondary unknowns without the normal displacement discontinuity.

With all the above definitions, the following relation for $n \geqslant 3$ is obtained:

$$\tilde{v}^2 = -\left(\tilde{\tilde{\kappa}}^2\right)^{-1}.\tilde{\kappa}^3.v^{k,k+1} \tag{A.19}$$

According to (A.19) and by defining:

$$\Psi^v = -\tilde{\kappa}^4.\left(\left(\tilde{\tilde{\kappa}}^2\right)^{-1}.\tilde{\kappa}^3\right) + \kappa_{k,k} \tag{A.20}$$

the interface k out-of-plane behavior Eq. (2.18) becomes for $n \geqslant 3$:

$$\gamma_z^{k,k+1} = \psi^v v^{k,k+1} \tag{A.21}$$

and for $n = 2$, the interface $k = 1$ out-of-plane behavior Eq. (2.18) gives:

$$\gamma_z^{1,2} = \frac{13}{35}(e^1S_v^1 + e^2S_v^2)v^{1,2} \tag{A.22}$$

Thus, the aimed relation is obtained for $n \geqslant 2$.

References

Allix, O., Ladevèze, P., 1992. Interlaminar interface modelling for the prediction of delamination. Compos. Struct. 22 (4), 235–242.

Allix, O., Lévéque, D., Perret, L., 1998. Identification and forecast of delamination in composite laminates by an interlaminar interface model. Compos. Sci. Technol. 58 (5), 671–678.

Andersons, J., König, M., 2004. Dependence of fracture toughness of composite laminates on interface ply orientations and delamination growth direction. Compos. Sci. Technol. 64 (13–14), 2139–2152.

Barbero, E., Reddy, J., 1991. Modeling of delamination in composite laminates using a layer-wise plate theory. Int. J. Solids Struct. 28 (3), 373–388.

Benzeggagh, M., Kenane, M., 1996. Measurement of mixed-mode delamination fracture toughness of unidirectional glass/epoxy composites with mixed-mode bending apparatus. Compos. Sci. Technol. 56 (4), 439–449.

Borg, R., Nilsson, L., Simonsson, K., 2002. Modeling of delamination using a discretized cohesive zone and damage formulation. Compos. Sci. Technol. 62 (10–11), 1299–1314.

Brewer, J., Lagace, P., 1988. Quadratic stress criterion for initiation of delamination. J. Compos. Mater. 22 (12), 1141–1155.

Bruno, D., Greco, F., Lonetti, P., 2005. A 3d delamination modelling technique based on plate and interface theories for laminated structures. Eur. J. Mech A/Solids 24 (1), 127–149.

Camanho, P., Dávila, C., De Moura, M., 2003. Numerical simulation of mixed-mode progressive delamination in composite materials. J. Compos. Mater. 37 (16), 1415–1438.

Caron, J., Diaz, A.D., Carreira, R., Chabot, A., Ehrlacher, A., 2006. Multi-particle modelling for the prediction of delamination in multi-layered materials. Compos. Sci. Technol. 66 (6), 755–765.

Carreira, R., Caron, J., Diaz, A.D., 2002. Model of multilayered materials for interface stresses estimation and validation by finite element calculations. Mecha. Mater. 34 (4), 217–230.

Carrera, E., 2004. On the use of the murakami's zig-zag function in the modeling of layered plates and shells. Comput. Struct. 82 (7–8), 541–554.

Chattopadhyay, J., Gu, H., 1994. A new higher-order plate theory in modeling delamination buckling of composite laminates. Am. Inst. Aeronaut. Astronaut. J. 32, 1709–1718.

Cho, M., 2001. Higher-order zig-zag theory for laminated composites with multiple delaminations. J. Appl. Mech. Trans. ASME 68 (6), 869–877.

Dallot, J., Sab, K., 2008. Limit analysis of multi-layered plates. Part II: shear effects. J. Mech. Phys. Solids 56 (2), 581–612.

Davidson, B., 1990. An analytical investigation of delamination front curvature in double cantilever beam specimens. J. Compos. Mater. 24, 1124–1137.

Davidson, B., Krüger, R., König, M., 1996. Effect of stacking sequence on energy release rate distributions in multidirectional DCB and ENF specimens. Eng. Fract. Mech. 55 (4), 557–569.

Davies, P., Blackman, B., Brunner, A., 2001. Mode II delamination. In: Moore, D.R., Pavan, A., Williams, J. (Eds.), Fracture Mechanics Testing Methods for Polymers, Adhesives and Composites, European Structural Integrity Society, vol. 28. Elsevier, pp. 307–333.

Diaz, A.D., Caron, J.-F., 2006a. Interface plasticity and delamination onset prediction. Mechanics of Materials 38 (7), 648–663.

Diaz, A.D., Caron, J.-F., 2006b. Prediction of the onset of mode III delamination in carbon-epoxy laminates. Compos. Struct. 72 (4), 438–445.

Diaz, A.D., Caron, J.-F., Carreira, R.P., 2002. Software application for evaluating interfacial stresses in inelastic symmetrical laminates with free edges. Compos. Struct. 58 (2), 195–208.

Diaz, A.D., Caron, J.-F., Ehrlacher, A., 2007. Analytical determination of the modes I, II and III energy release rates in a delaminated laminate and validation of a delamination criterion. Compos. Struct. 78 (3), 424–432.

Ducept, F., Gamby, D., Davies, P., 1999. A mixed-mode failure criterion derived from tests on symmetric and asymmetric specimens. Compos. Sci. Technol. 59 (4), 609–619.

Duong, V.A., Diaz, A.D., Chataigner, S., Caron, J.-F., 2011. A layerwise finite element for multilayers with imperfect interfaces. Compos. Struct. 93 (12), 3262–3271.

Greco, F., Lonetti, P., Zinno, R., 2002. An analytical delamination model for laminated plates including bridging effects. Int. J. Solids Struct. 39 (9), 2435–2463.
Harper, P.W., Hallett, S.R., 2008. Cohesive zone length in numerical simulations of composite delamination. Eng. Fract. Mech. 75 (16), 4774–4792.
Hashemi, S., Kinloch, A.J., Williams, J.G., 1990. The analysis of interlaminar fracture in uniaxial fibre-polymer composites. Proc. R. Soc. Lond. A 427, 173–199.
Hochard, C., Lahellec, N., Bordreuil, C., 2007. A ply scale non-local fibre rupture criterion for CFRP woven ply laminated structures. Compos. Struct. 80 (3), 321–326.
Hwang, C., Wawrzynek, P., Tayebi, A., Ingraffea, A., 1998. On the virtual crack extension method for calculation of the rates of energy release rate. Eng. Fract. Mech. 59 (4), 521–542.
Irwin, G., 1957. Analysis of stress and strains near the end of a crack traversing a plate. J. Appl. Mech. 24 (3), 361–364.
Kim, H.S., Chattopadhyay, A., Ghoshal, A., 2003. Characterization of delamination effect on composite laminates using a new generalized layerwise approach. Comput. Struct. 81 (15), 1555–1566.
Kinloch, A., Wang, Y., Williams, J., Yayla, P., 1993. The mixed-mode delamination of fibre composite materials. Compos. Sci. Technol. 47 (3), 225–237.
Krueger, R., 2004. Virtual crack closure technique: history, approach, and applications. Appl. Mech. Rev. 57 (2), 109–143.
Lachaud, F., Lorrain, B., Michel, L., Barriol, R., 1998. Experimental and numerical study of delamination caused by local buckling of thermoplastic and thermoset composites. Compos. Sci. Technol. 58 (5), 727–733.
Larsson, P.-L., 1991. On multiple delamination buckling and growth in composite plates. Int. J. Solids Struct. 27 (13), 1623–1637.
Lee, J., 2000. Free vibration analysis of delaminated composite beams. Comput. Struct. 74 (2), 121–129.
Moorthy, C.D., Reddy, J., 1998. Modeling of delamination using a layerwise element with enhanced strains. In: Damage Mechanics in Engineering Materials. Studies in Applied Mechanics, vol. 46. Elsevier, pp. 459–479.
Murakami, H., 1986. Laminated composite plate theory with improved in-plane responses. J. Appl. Mech. 53, 661–666.
Naciri, T., Ehrlacher, A., Chabot, A., 1998. Interlaminar stress analysis with a new multiparticle modelization of multilayered materials (M4). Compos. Sci. Technol. 58 (3–4), 337–343.
Nguyen, V.-T., Caron, J.-F., 2006. A new finite element for free edge effect analysis in laminated composites. Comput. Struct. 84 (22–23), 1538–1546.
Nilsson, K.-F., 1993. On growth of crack fronts in the DCB-test. Compos. Eng. 3 (6), 527–546.
Oh, J., Cho, M., Kim, J.-S., 2008. Buckling analysis of a composite shell with multiple delaminations based on a higher order zig-zag theory. Finite Elem. Anal. Des. 44 (11), 675–685.
Orifici, A., Herszberg, I., Thomson, R., 2008. Review of methodologies for composite material modelling incorporating failure. Compos. Struct. 86 (1–3), 194–210.
Ousset, Y., 1999. Numerical simulation of delamination growth in layered composite plates. Eur. J. Mech. A/Solids 18 (2), 291–312.
Pagano, N., 1978. Stress fields in composite laminates. Int. J. Solids Struct. 14 (5), 385–400.
Prombut, P., Michel, L., Lachaud, F., Barrau, J., 2006. Delamination of multidirectional composite laminates at $0^\circ/\theta^\circ$ ply interfaces. Eng. Fract. Mech. 73 (16), 2427–2442.
Qiu, Y., Crisfield, M., Alfano, G., 2001. An interface element formulation for the simulation of delamination with buckling. Eng. Fract. Mech. 68 (16), 1755–1776.
Reissner, E., 1950. On a variational theorem in elasticity. J. Math. Phys. 29 (2), 90–95.
Rice, J., 1968. A path independent integral and the approximate analysis of strain concentration by notches and cracks. J. Appl. Mech. 35 (2), 379–386.
Saeedi, N., Sab, K., Caron, J.-F., 2012a. Delaminated multilayered plates under uniaxial extension. Part I: analytical analysis using a layerwise stress approach. Int. J. Solids Struct. 49 (26), 3711–3726.
Saeedi, N., Sab, K., Caron, J.-F., 2012b. Delaminated multilayered plates under uniaxial extension. Part II: efficient layerwise mesh strategy for the prediction of delamination onset. Int. J. Solids Struct. 49 (26), 3727–3740.
Shen, M.-H., Grady, J., 1992. Free vibrations of delaminated beams. AIAA J. 30 (5), 1361–1370.
Sun, C., Zheng, S., 1996. Delamination characteristics of double-cantilever beam and end-notched flexure composite specimens. Compos. Sci. Technol. 56 (4), 451–459.
Szekrenyes, A., 2013a. Analysis of classical and first-order shear deformable cracked orthotropic plates. J. Compos. Mater.
Szekrenyes, A., 2013b. Interface fracture in orthotropic composite plates using second-order shear deformation theory. Int. J. Damage Mech.
Tan, S., 1988. Effective stress fracture models for unnotched and notched multidirectional laminates. J. Compos. Mater. 22 (4), 322–340.
Thai, N.D., D'Ottavio, M., Caron, J.-F., 2013. Bending analysis of laminated and sandwich plates using a layer-wise stress model. Compos. Struct. 96, 135–142.
Vandellos, T., Huchette, C., Carrère, N., 2013. Proposition of a framework for the development of a cohesive zone model adapted to carbon-fiber reinforced plastic laminated composites. Compos. Struct. 105, 199–206.
Whitney, J., Nuismer, R., 1974. Stress fracture criteria for laminated composites containing stress concentrations. Compos. Sci. Technol. 8, 253–265.
Williams, J., 1989. Fracture mechanics of delamination tests. J. Strain Anal. Eng. Des. 24 (4), 207–214.
Wu, E.M., Reuter, R.C., 1965. Crack extension in fiberglass reinforced plastics. T. & AM Report University of Illinois (275).
Yu, L., Davidson, B.D., 2001. A three-dimensional crack tip element for energy release rate determination in layered elastic structures. J. Compos. Mater. 35 (6), 457–488.
Zhang, J., Fan, J., Herrmann, K., 1999. Delaminations induced by constrained transverse cracking in symmetric composite laminates. Int. J. Solids Struct. 36 (6), 813–846.
Zou, Z., Reid, S., Li, S., Soden, P., 2002. Application of a delamination model to laminated composite structures. Compos. Struct. 56 (4), 375–389.